Hindawi Publishing Corporation
International Journal of Photoenergy
Volume 2012, Article ID 171432, 8 pages
doi:10.1155/2012/171432

*Research Article*

# Electrochemical Deposition of $Cu_xSn_yS_zO$ Thin Films and Their Application for Heterojunction Solar Cells

**Yuki Nakashima and Masaya Ichimura**

*Department of Engineering Physics, Electronics and Mechanics, Nagoya Institute of Technology, Gokiso, Showa, Nagoya 466-8555, Japan*

Correspondence should be addressed to Masaya Ichimura, ichimura.masaya@nitech.ac.jp

Received 11 July 2011; Accepted 26 November 2011

Academic Editor: Peter Rupnowski



$Cu_xSn_yS_zO$ (CTSO) thin films were deposited from an aqueous solution containing $CuSO_4$, $SnSO_4$, and $Na_2S_2O_3$ by electrochemical techniques. The deposited films were characterized by Auger electron spectroscopy, X-ray diffraction, and optical transmission spectroscopy. The photoelectrochemical measurement showed that the films have p-type conduction and photosensitivity. ZnO/CTSO heterojunction solar cells were fabricated. Rectification properties were observed, and the cell showed an efficiency of $4.9 \times 10^{-3}$% under AM1.5 illumination.

## 1. Introduction

For heterojunction solar cells, compound semiconductors composed of cheap and nontoxic elements are strongly desired. For an absorption layer, CdTe and $CuInSe_2$ are popular but their constituent elements are toxic (Cd, Se) or not abundant (Te, In, Se). $Cu_xO$ ($x$ = 1,2) and SnS are considered as promising because of their suitable band gap and p-type conduction. In addition, their constituent elements are all nontoxic and abundant. There are several reports on solar cells based on $Cu_xO$ [1–4] and SnS [5–10]. Their thin films have been deposited by various techniques, such as evaporation, spray pyrolysis, chemical techniques, and sulfurization or oxidation of metal, and the highest efficiency reported so far is about 1.3% for both the materials [1, 7]. Recently, $Cu_2ZnSnS_4$ was successfully applied for the absorber layer [11, 12], which has evoked interest for new multinary compounds and alloys with a narrow band gap and p-type conduction.

In this paper, we deposit a quaternary alloy $Cu_xSn_yS_zO$ (CTSO) and apply it for solar cells for the first time. CTSO can be considered as a mixture of $Cu_xO$ and SnS, and we may be able to tune its properties by controlling the composition values $x$, $y$, and $z$. Thus CTSO will be potentially advantageous for absorption layers of heterojunction solar cells. To deposit CTSO films, we adopted electrochemical techniques. Electrochemical deposition (ECD) is a low-cost, simple technique, and suitable for large-scale deposition. It has been successfully used to deposit various semiconductors including $Cu_xO$ [13–15] and SnS [16–18]. As a partner of CTSO in the heterojunction (the window or buffer layer), we selected ZnO. ECD of ZnO was well established [19, 20], and successful fabrication of ZnO/$Cu_2O$ [21–23] and ZnO/SnS [24] solar cells by the electrochemical techniques has been reported. Therefore, ECD fabrication of ZnO/CTSO heterojunction solar cells is worth attempting. To discuss their solar cell characteristics, we evaluate the band offset at the ZnO/CTSO heterojunction using X-ray photoelectron spectroscopy (XPS).

## 2. Experimental Procedure

*2.1. Film Deposition and Characterizations.* For the $Cu_xSn_yS_zO$ deposition, we used an aqueous solution containing $CuSO_4$, $SnSO_4$, and $Na_2S_2O_3$. $CuSO_4$ concentration was set 10 mM and $Na_2S_2O_3$ concentration 100 mM, and $SnSO_4$ concentration was varied. pH was about 3 (unadjusted), and the solution amount is 50 mL. In an acidic

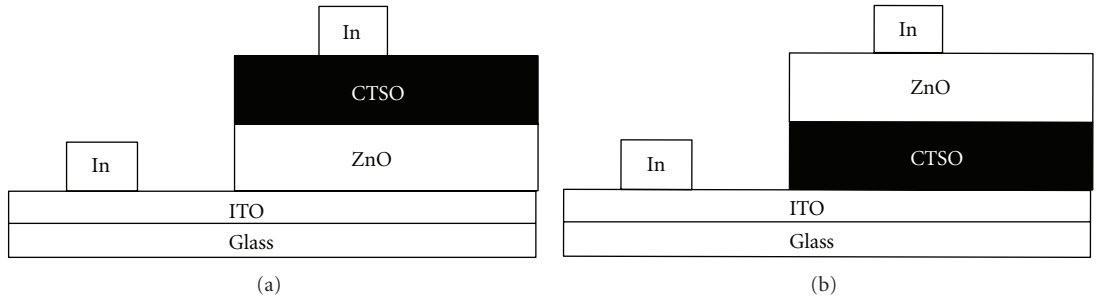


Figure 1: Schematic illustrations of (a) the CTSO/ZnO superstrate heterostructure and (b) the ZnO/CTSO substrate heterostructure. For the substrate structure (b), the light should be incident on the ZnO side through a transparent electrode. However, since the metal electrode was deposited on ZnO, the light was incident on the substrate side in the measurement.

solution, $S_2O_3^{2-}$ ions are expected to release S atoms by the following reaction [25]:

$$2H^+ + S_2O_3^{2-} = S + H_2SO_3. \quad (1)$$

The deposition solution was hazy because of sulfur colloids formed by the above reaction. A three-electrode cell was used with a saturated calomel electrode (SCE) as the reference electrode, an indium-tin-oxide (ITO)-coated glass sheet as the working electrode, and a platinum sheet as the counter electrode. The deposition potential is determined by cyclic voltametry (CV). By CV, we study the current response of the electrochemical system under the application of a triangular potential sweep. The cathodic scan is from 0 to −1.5 V versus SCE, and the anodic scan is from −1.5 to +0.5 V versus SCE with a scan rate of 20 mV/s. The compositional analysis was carried out by Auger electron spectroscopy (AES) using the model JEOL JAMP 7800 Auger microprobe at probe voltage 10 kV and current $2 \times 10^{-8}$ A. An argon-ion sputtering with an acceleration voltage of 3 kV and a current of 20 mA was used to sputter the film surface. The $x$, $y$, and $z$ values were calculated using standard $Cu_2S$, SnS, CuO, and $SnO_2$ compounds. Profile meter Accretech Surfcom-1400D was used to measure the thickness of the film. The surface morphology of the film was analyzed by scanning electron microscope (SEM, Hitachi S-2000S), keeping the acceleration voltage at 10 kV. The X-ray diffraction (XRD) measurement was carried out with the RIGAKU RINT-2000 diffractometer using Cu K$\alpha_1$ radiation. Furthermore, the photoconductivity of the film was examined by means of the photoelectrochemical (PEC) measurements. The PEC measurement was carried out using the same three-electrode cell as that used for the deposition. The deposited film was used as the working electrode, and a solution containing 100 mM $Na_2S_2O_3$ was used for the electrolyte. The backside of the sample was illuminated by pulsed light coming from an Xe lamp. The incident light was turned off and on mechanically every five seconds by putting and removing a barrier between the lamp and the sample, respectively [16, 17, 26]. The potential applied to the working electrode was scanned linearly first in the cathodic potential range (from 0 to −1 V versus SCE) and then the anodic potential range (from 0 to +1 V versus SCE).

*2.2. Heterostructure Fabrication and Characterization.* For any heterostructure solar cell, one can consider two different geometries, that is, superstrate and substrate structures. Thus we attempted to fabricate both the types of cells shown in Figure 1. Indium metal electrodes were deposited by thermal evaporation. The electrode size is 1 $mm^2$ and the distance between electrodes is 1 mm. ZnO was also deposited by the electrochemical technique. For the ZnO deposition, we used a solution containing 100 mM zinc nitrate [19]. The deposition temperature was 313 K. The deposition potential was a two-step pulse with $E_1 = -1.3$ V versus SCE, $E_2 = -0.6$ V versus SCE, and each pulse duration was 10 s. The deposition time was 3 min. For the photovoltaic characterization, current-voltage ($I$-$V$) characteristics were measured in the dark and under illumination. An Xe lamp with an AM1.5 radiation filter was used as the light source, and its radiation power was about 100 mW/$cm^2$. The glass side of the sample was illuminated for all the samples. For the substrate structure cell, the ZnO side should in fact be irradiated. However, we are not able to deposit transparent electrode but only a metal electrode on ZnO. Thus, since the ZnO side surface is shielded by the metal electrode, the substrate side was illuminated.

The band offset was evaluated using XPS PHI-5000 (ULVAC-PHI). The XPS spectra were measured using the Al K$\alpha$ line as an X-ray source. We adopted the core-level spectroscopy technique [27]: we first measured the valence band maximum (VBM) with respect to the metal 3d or 4d level for the individual layer, and then measured the core level difference at the heterointerface by removing the upper layer by Ar-ion sputtering.

## 3. Results and Discussion

*3.1. CTSO Films Deposition.* We varied concentration of $SnSO_4$ from 3 to 30 mM as shown in Table 1. Figure 2 shows CV results for the solutions of condition 1 (3 mM $SnSO_4$) and condition 5 (30 mM $SnSO_4$). In the negative scans, reduction current peaks appeared, and we adopted the deposition potential around the reduction peak potential.

First, we attempted deposition using DC bias in all the solution conditions, keeping the deposition time 30 min. We obtained thin films except for the 30 mM $SnSO_4$ condition,

Table 1: Deposition conditions and the corresponding film thickness and composition. $CuSO_4$ concentration was 10 mM and $Na_2S_2O_3$ concentration 100 mM. Data in the parentheses are for the film fabricated by 5 min deposition. All other data are for the 30-min-deposited films. The deposition potential of condition 5 is a two-step pulse potential with $E_1 = -1.3$ V versus SCE, $E_2 = -0.6$ V versus SCE, and each pulse duration was 10 s.

| | $SnSO_4$ [mM] | Deposition potential [$V$ versus SCE] | Thickness [$\mu$m] | Cu : Sn : S : O |
|---|---|---|---|---|
| Condition 1 | 3 | −0.80 | 0.50<br>(0.15) | 1.7 : 0.084 : 0.13 : 1.0<br>(2.5 : 0.47 : 0.52 : 1.0) |
| Condition 2 | 6 | −0.82 | 0.30 | 2.1 : 0.50 : 0.60 : 1.0 |
| Condition 3 | 9 | −0.85 | 0.35 | 2.1 : 0.49 : 0.79 : 1.0 |
| Condition 4 | 12 | −0.87 | 0.30 | 2.6 : 0.71 : 0.90 : 1.0 |
| Condition 5 | 30 | two-step pulse | 2.5 | 0.97 : 0.68 : 1.3 : 1.0 |

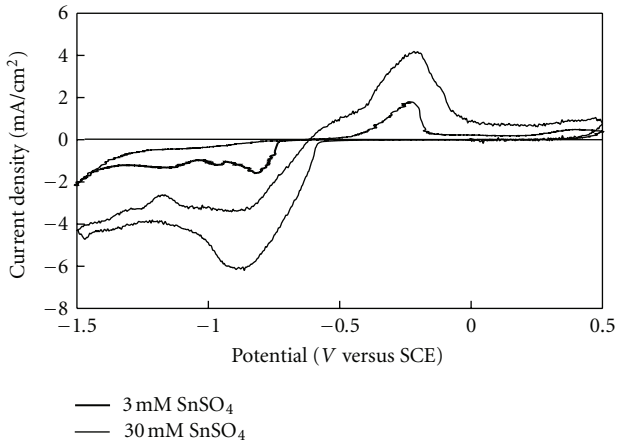


Figure 2: Cyclic voltametry results for the solutions containing 3 mM and 30 mM $SnSO_4$.

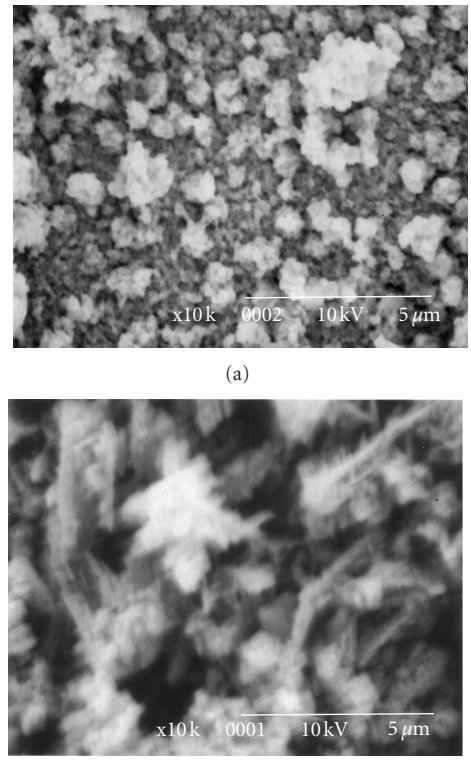


Figure 3: SEM images of the films deposited under condition 1 (a) and condition 5 (b). The former one is denser than the latter.

where the adhesion was so poor that a film was not formed on the substrate. Thus, we applied a two-step pulse potential with $E_1 = -1.3$ V versus SCE, $E_2 = -0.6$ V versus SCE, and pulse duration of 10 s (condition 5). The effects of the pulse biasing with such a long pulse duration were discussed in our previous paper for SnS deposition [18]. During the "off" period, poorly deposited parts are thought to dissolve, resulting in better surface morphology. The pulse biasing in fact improved adhesion for condition 5, but the surface morphology was not improved sufficiently, as shown below. In preparatory experiments, we found that the pulse biasing is not effective for improving morphology of $Cu_xS$ films. Thus we did not try the pulse-biasing deposition for the Cu-rich conditions (conditions 1–4).

Table 1 also shows the thickness and composition of the films. From the table, we can see that as the $SnSO_4$ concentration was increased, both Sn and S contents were increased. The oxygen content is larger than or comparable to the sulfur content. The source of the oxygen in the films would be dissolved oxygen in the solution since we did not purge oxygen before the deposition.

Figure 3 shows the SEM images of the films deposited under condition 1 (Figure 3(a)) and condition 5 (Figure 3(b)). The film deposited under condition 1 seems more compact than that deposited under condition 5, and the growth seems to be dendritic for deposition under condition 5. In our previous work, we deposited SnS using 30 mM $SnSO_4$ and 100 mM $Na_2S_2O_3$ as in condition 5 [18]. Films deposited using DC potential were porous, but those deposited using a pulse bias were much more compact. However, in the present case, the film deposited using a pulse bias (condition 5) is porous as shown in Figure 3(b), and therefore the pulse biasing is not so effective to improve the morphology in case of CTSO.

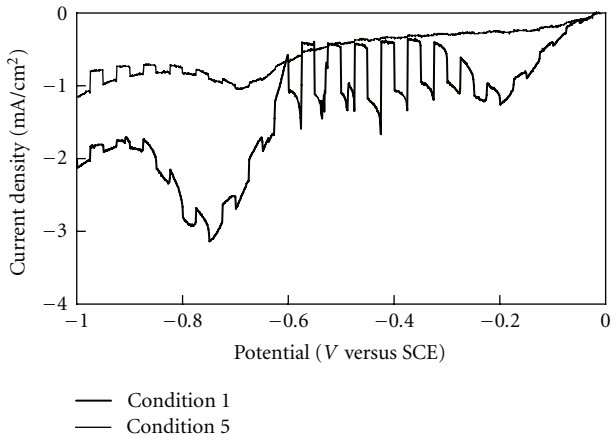


Figure 4: Results of the PEC measurement for the films deposited under condition 1 and condition 5. The step-form variation in the current is due to the turning on/off of the illumination. The observed photocurrent is negative for both the samples.

To investigate the photosensitivity of the deposited films, we performed the PEC measurement. Figure 4 shows the results of the PEC measurement for condition 1 and condition 5. The current was not changed by illumination for the anodic scan, and thus only the results for the cathodic scan are shown in the figure. During the cathodic scan, the current was changed due to the light chopping. When the junction of the semiconductor-electrolyte is illuminated, photogenerated electrons/holes are separated in the space charge region. The photogenerated minority carriers arrive at the interface of the semiconductor-electrolyte to participate in the electrochemical reaction at the film/electrolyte interface. The current becomes more negative under the light illumination during the cathodic scan. This implies that the minority carriers generated here are electrons. Thus, the deposited films are p-type. The photocurrent for the film deposited under condition 1 is bigger than those for the other condition films. Therefore, we adopt condition 1 for fabrication of the solar cells. The poor photoresponse of the film deposited under condition 5 would partly be due to the porous nature of the film (see Figure 3).

The color of the deposition solution changed with time because of spontaneous chemical reactions. To investigate dependence of film properties on deposition time, we changed deposition time from 30 to 5 min. The composition and thickness of the film obtained by 5 min deposition under condition 1 were shown in the parentheses in Table 1. It can be seen that Sn and S contents are larger for the shorter deposition time. The average deposition rate is also larger for the initial 5 min (0.03 $\mu$m/min) than for the 30 min deposition (0.017 $\mu$m/min). We may consider that Sn and S reacted in the solution to form SnS colloidal particles, resulting in decrease in Sn and S contents in the film and also decrease in deposition rate for a longer deposition time.

The XRD spectra of the films deposited under condition 1 are shown in Figure 5 with the spectrum for the ITO glass substrate. The observed peaks are all attributed to the ITO substrate for the 5 min deposition sample, whereas a broad peak appears near $2\theta = 43^\circ$ for the 30 min deposition sample. We could not identify the broad peak since its $2\theta$ value does not correspond to those of the dominant peaks of related binary compounds ($SnS_x$, $Cu_xO$, $x$ = 1 or 2). Since SnS and $Cu_2O$ films deposited by ECD exhibited clear diffraction peaks [18, 21], the absence of clear diffraction peaks indicates that the CTSO films are amorphous or nanocrystalline and do not include those separate binary phases.

For estimating the band gap, we measured the optical transmission of CTSO. Figure 6 shows the optical transmission of the CTSO film deposited under condition 1 with a deposition time of 5 min. The transmission is low in the whole range obviously because of scattering due to the rough surface morphology (Figure 3). A clear absorption edge did not appear, which will be due to amorphous or nanocrystalline nature of the film revealed by XRD (Figure 5). For the direct-band optical absorption, the absorption coefficient $\alpha$ is given by

$$\alpha = \frac{k\left(h\nu - E_g\right)^{1/2}}{h\nu}, \tag{2}$$

where $k$ is a constant, $E_g$ the band gap, and $h\nu$ the photon energy. Figure 7 shows $h\nu$ versus $(\alpha h\nu)^2$ plot. There is no clear straight-line portion in the plot, and $\alpha$ begins to increase gradually around 1 eV and then more steeply around 1.5 eV. Thus, the band gap would be in a range between 1 and 1.5 eV.

*3.2. Heterojunction Solar Cells.* We attempted to fabricate the superstrate and substrate heterojunctions with ZnO as a window layer and CTSO as an absorption layer. In case of the superstrate heterojunction, we found that the underlying ZnO layer was dissolved during the subsequent CTSO deposition. The same problem was also reported for the SnS deposition on ZnO [24]. Recently, a buffering method was proposed to prevent dissolution of ZnO during deposition of $Cu_2O$ on it [28]. A suitable amount of ZnO is dissolved into the $Cu_2O$ deposition solution, and then stability of ZnO can be improved. This method is effective for alkaline solutions because the solubility of $HZnO_2^-$, the product of ZnO dissolution, is relatively low. In the present case, pH of the CTSO deposition solution is about 3, and the solubility of $Zn^{2+}$, the product of ZnO dissolution in acidic solutions, is quite high. Thus the ZnO dissolution could not be prevented by the buffering technique. Therefore, we actually fabricated the substrate heterojunction only. Figure 8 shows the dark $I$-$V$ characteristics for the substrate heterojunction with the 30-min-deposited CTSO layer. The rectification property appeared, but we did not find any photovoltaic effects.

In the substrate structure, the light is incident on the CTSO (absorption layer) side, and thus the light is attenuated before reaching the pn junction region. This would be the main reason why the photocurrent was not observed for the 30-min-deposited CTSO layer, and thus we reduced the CTSO film thickness. Figure 9 shows the dark and illuminated $I$-$V$ characteristics for the substrate heterojunction with the 5-min-deposited CTSO layer. We

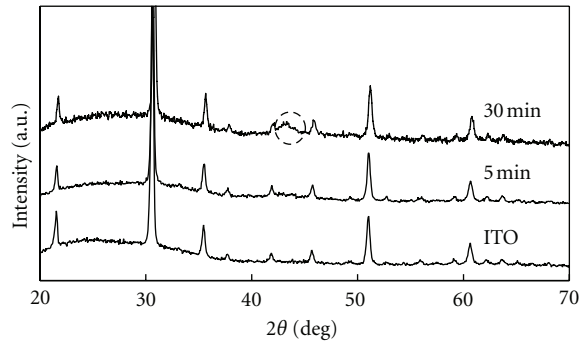


Figure 5: XRD spectra for the CTSO films deposited under condition 1 with different deposition time (5 min and 30 min). A broad peak near $2\theta = 43^\circ$ observed for the 30 min deposition sample (the circle in the figure) can be attributed to the CTSO film, and all other peaks are due to ITO.

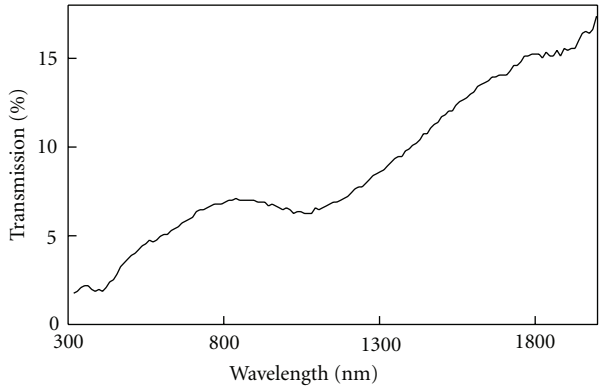


Figure 6: Optical transmission of the CTSO film deposited under condition 1 for 5 min.

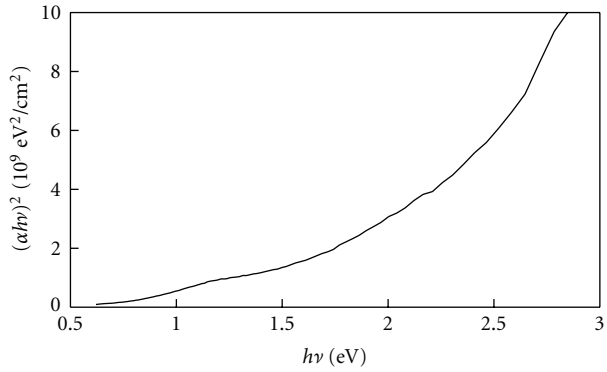


Figure 7: Plot of the absorption coefficient for band gap estimation of the CTSO film deposited under condition 1.

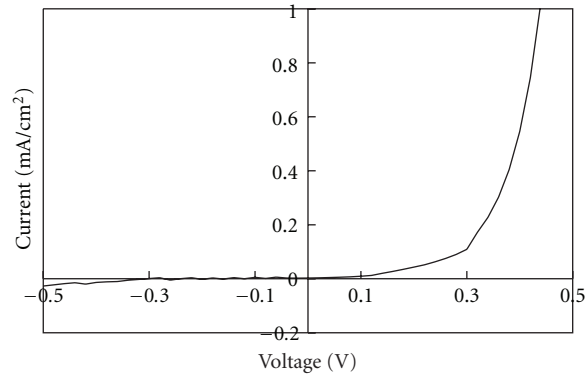


Figure 8: Dark $I$-$V$ characteristic for the substrate heterojunction with the 30-min-deposited CTSO film (condition 1).

confirmed rectification and photovoltaic effects. The conversion efficiency of the best cell was $4.9 \times 10^{-3}$% with $V_{oc}$ of 0.165 V, $I_{sc}$ of 0.1 mA/cm$^2$, and FF of 0.30. The efficiency is significantly lower than those of SnS- and $Cu_2O$-based solar cells, for which efficiency values larger than 1% were reported [1, 7]. It should be noted that while those previously reported cells were all superstrate-structure cells, the cell fabricated in this work is of the substrate structure as noted above. Thus the observed poor photovoltaic properties will be mainly due to the cell structure (substrate structure). Another possible reason for the poor properties could be poor crystallinity of CTSO. Since there are no sharp diffraction peaks in the XRD spectra shown in Figure 5, the CTSO films are considered to be amorphous or nanocrystalline. Then the carrier diffusion length will be very short. On the other hand, clear diffraction peaks are observed for ECD SnS and $Cu_2O$, as mentioned above, and thus the diffusion length may be longer in them than in CTSO. To improve the performance, annealing may be effective and will be attempted in a future study. Properties of the heterointerface are another important factor and thus will be discussed in the next subsection.

*3.3. Band Offsets.* For the ZnO/CTSO cells, we confirmed photovoltaic effects, but the short-circuit current was small. The band offset at the interface is one of the most influential parameters for the efficiency of the heterojunction solar cells. Thus, to discuss the observed solar cell properties, the XPS technique was used to determine the band offset of the prepared junction. For the ZnO/CTSO structure, the valence-band offset $\Delta E_v$ is given by the equation

$$\Delta E_v = \Delta E^{\text{CTSO}}_{\text{VBM-Sn}} - \Delta E^{\text{ZnO}}_{\text{VBM-Zn}} - \Delta E_{\text{Zn-Sn}}, \tag{3}$$

where $\Delta E^{\text{CTSO}}_{\text{VBM-Sn}}$ is the energy separation between the valence-band maximum (VBM) and the Sn4d core level for CTSO, $\Delta E^{\text{ZnO}}_{\text{VBM-Zn}}$ the separation between VBM and the Zn3d core level for ZnO, $\Delta E_{\text{Zn-Sn}}$ the energy difference across the interface between the Sn4d core level in the CTSO side, and the Zn3d core level in the ZnO side of the junction. Figure 10 shows the XPS spectra of CTSO (deposited under condition 1) and ZnO. The VBM positions were deduced by linear extrapolation of the leading edge of the expanded spectra, as shown in Figure 10(b), and the first and second terms of (3) were obtained as follows:

$$\begin{aligned} \Delta E^{\text{CTSO}}_{\text{VBM-Sn}} &= 25.25\,\text{eV}, \\ \Delta E^{\text{ZnO}}_{\text{VBM-Zn}} &= 8.1\,\text{eV}. \end{aligned} \tag{4}$$

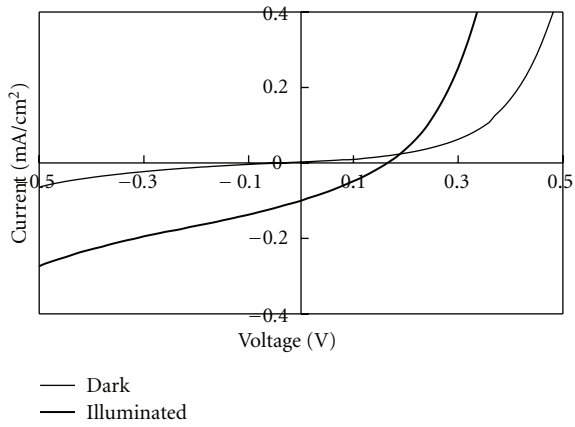


Figure 9: Dark and illuminated $I$-$V$ characteristics for the substrate heterojunction with the 5-min-deposited CTSO film (condition 1).

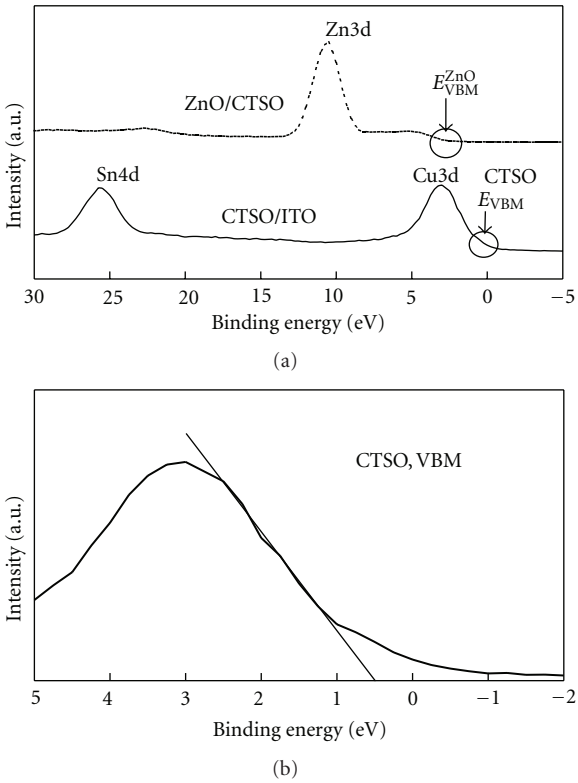


Figure 10: (a) XPS spectra for the ZnO and CTSO films. The CTSO film was deposited under condition 1. (b) expanded spectrum near VBM for CTSO. The straight line in (b) is the linear extrapolation of the leading edge, and the intercept on the energy axis corresponds to the VBM position.

Figure 11 shows the XPS spectra for the interface between CTSO and ZnO. The three spectra were taken with different sputtering time to determine the position of each peak. From this result, we estimated

$$\Delta E_{\text{Zn-Sn}} = 15.25\,\text{eV}. \tag{5}$$

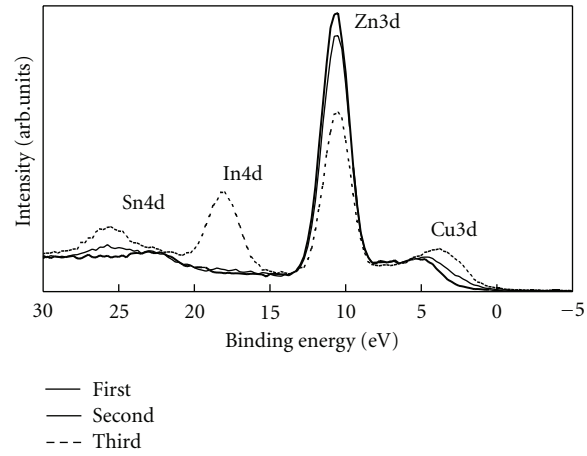


Figure 11: XPS spectra of Sn4d and Zn3d core levels near the ZnO/CTSO interface taken with three different sputtering times.

On the basis of (3), we calculated $\Delta E_v$ as 1.9 eV. The conduction-band offset $\Delta E_c$ was calculated using the band gap of each material as

$$\Delta E_c = \left(E_g^{\text{ZnO}} - E_g^{\text{CTSO}}\right) - \Delta E_v. \tag{6}$$

The band gap of ZnO is 3.4 eV. As described above, we were not able to accurately evaluate the band gap of CTSO from the optical transmission measurement, and $E_g^{\text{CTSO}}$ was only roughly estimated to be in a range of 1 to 1.5 eV. Figure 12 shows the schematic of the band alignment estimated from the XPS results. Considering the ambiguity of the band gap value, the band edges of CTSO were indicated by the thick lines with a width corresponding to 0.25 eV. As shown in the figure, even if we consider the uncertainty of the band gap of CTSO, we may conclude that the conduction band offset will be small. In that case, we can expect that the short circuit current will be relatively large since there is only a low barrier for the electron flow. However, the ZnO/CTSO cell showed a small short circuit current. As discussed in the previous section, the cell geometry (substrate structure) and the short diffusion length of carriers in CTSO may be the reason of the low efficiency. Another possible reason is that ZnO and CTSO were mixed at the heterojunction interface, to form an interface layer which hinders the electron flow. As shown in Figure 11, the transition of composition from ZnO to CTSO is not sharp, that is, the Zn signal is still significant even after the Cu and Sn signals appear. This may be partly due to the roughness of the surface/interface and partly due to the atomic mixing at the interface. Thus, heterostructures with other materials than ZnO also need to be investigated.

## 4. Conclusion

Using the electrochemical techniques, $Cu_xSn_yS_zO$ (CTSO) thin films have been deposited from an aqueous solution containing $CuSO_4$, $SnSO_4$, and $Na_2S_2O_3$. The $CuSO_4$ and $Na_2S_2O_3$ concentrations were fixed at 10 mM and 100 mM, respectively, while the $SnSO_4$ concentration was varied. The

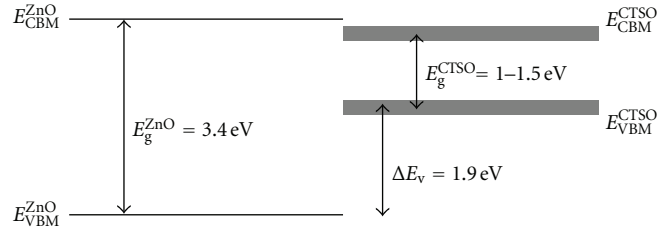


Figure 12: Band diagram of the ZnO/CTSO heterojunction deduced form the XPS results.

deposited films showed clear p-type conduction and photosensitivity. The film deposited with the solution containing 10 mM $CuSO_4$, 3 mM $SnSO_4$, and 100 mM $Na_2S_2O_3$ has a band gap of 1.0–1.5 eV and seems to be nanocrystalline or amorphous according to the XRD results. The film was used for fabricating ZnO/CTSO heterojunctions. Rectification properties were observed, and the best cell showed an efficiency of $4.9 \times 10^{-3}$% under AM1.5 illumination.

## Acknowledgments

The authors would like to thank Drs. M. Kato, A. M. Abdel Haleem, and S. Chowdhury for their useful discussion and Mr. Moriguchi for his technical assistance in the XPS measurement.

## References

[1] A. Mittiga, E. Salza, F. Sarto, M. Tucci, and R. Vasanthi, "Heterojunction solar cell with 2% efficiency based on a $Cu_2O$ substrate," *Applied Physics Letters*, vol. 88, no. 16, Article ID 163502, 2006.

[2] K. Akimoto, S. Ishizuka, M. Yanagita, Y. Nawa, G. K. Paul, and T. Sakurai, "Thin film deposition of $Cu_2O$ and application for solar cells," *Solar Energy*, vol. 80, no. 6, pp. 715–722, 2006.

[3] H. Tanaka, T. Shimakawa, T. Miyata, H. Sato, and T. Minami, "Electrical and optical properties of TCO-$Cu_2O$ heterojunction devices," *Thin Solid Films*, vol. 469-470, pp. 80–85, 2004.

[4] L. Papadimitriou, N. A. Economou, and D. Trivich, "Heterojunction solar cells on cuprous oxide," *Solar Cells*, vol. 3, no. 1, pp. 73–80, 1981.

[5] M. Gunasekaran and M. Ichimura, "Photovoltaic cells based on pulsed electrochemically deposited SnS and photochemically deposited CdS and $Cd_{1-x}Zn_xS$," *Solar Energy Materials and Solar Cells*, vol. 91, no. 9, pp. 774–778, 2007.

[6] H. Noguchi, A. Setiyadi, H. Tanamura, T. Nagatomo, and O. Omoto, "Characterization of vacuum-evaporated tin sulfide film for solar cell materials," *Solar Energy Materials and Solar Cells*, vol. 35, no. C, pp. 325–331, 1994.

[7] K. T. Ramakrishna Reddy, N. Koteswara Reddy, and R. W. Miles, "Photovoltaic properties of SnS based solar cells," *Solar Energy Materials and Solar Cells*, vol. 90, no. 18-19, pp. 3041–3046, 2006.

[8] D. Avellaneda, M. T. S. Nair, and P. K. Nair, "Photovoltaic structures using chemically deposited tin sulfide thin films," *Thin Solid Films*, vol. 517, no. 7, pp. 2500–2502, 2009.

[9] M. Ristov, G. Sinadinovski, M. Mitreski, and M. Ristova, "Photovoltaic cells based on chemically deposited p-type SnS," *Solar Energy Materials and Solar Cells*, vol. 69, no. 1, pp. 17–24, 2001.

[10] M. Sugiyama, K. Miyauchi, T. Minemura, and H. Nakanishi, "Sulfurization growth of SnS films and fabrication of CdS/SnS heterojunction for solar cells," *Japanese Journal of Applied Physics*, vol. 47, no. 12, pp. 8723–8725, 2008.

[11] H. Katagiri, K. Jimbo, S. Yamada et al., "Enhanced conversion efficiencies of $Cu_2ZnSnS_4$-based thin film solar cells by using preferential etching technique," *Applied Physics Express*, vol. 1, no. 4, Article ID 041201, 2008.

[12] K. Wang, O. Gunawan, T. Todorov et al., "Thermally evaporated $Cu_2$ $ZnSnS_4$ solar cells," *Applied Physics Letters*, vol. 97, no. 14, Article ID 143508, 2010.

[13] T. D. Golden, M. G. Shumsky, Y. Zhou, R. A. VanderWerf, R. A. Van Leeuwen, and J. A. Switzer, "Electrochemical deposition of copper(I) oxide films," *Chemistry of Materials*, vol. 8, no. 10, pp. 2499–2504, 1996.

[14] K. Nakaoka, J. Ueyama, and K. Ogura, "Photoelectrochemical behavior of electrodeposited CuO and $Cu_2O$ thin films on conducting substrates," *Journal of the Electrochemical Society*, vol. 151, no. 10, pp. C661–C665, 2004.

[15] J. Lee and Y. Tak, "Electrochemical deposition of a single phase of pure $Cu_2O$ films by current modulation methods," *Electrochemical and Solid-State Letters*, vol. 3, no. 2, pp. 69–72, 2000.

[16] K. Mishra, K. Rajeshwar, A. Weiss et al., "Electrodeposition and characterization of SnS thin films," *Journal of the Electrochemical Society*, vol. 136, no. 7, pp. 1915–1923, 1989.

[17] Z. Zainal, M. Z. Hussein, and A. Ghazali, "Cathodic electrodeposition of SnS thin films from aqueous solution," *Solar Energy Materials and Solar Cells*, vol. 40, no. 4, pp. 347–357, 1996.

[18] K. Omoto, N. Fathy, and M. Ichimura, "Deposition of $SnS_xO_y$ films by electrochemical deposition using three-step pulse and their characterization," *Japanese Journal of Applied Physics*, vol. 45, no. 3A, pp. 1500–1505, 2006.

[19] M. Izaki and T. Omi, "Characterization of transparent zinc oxide films prepared by electrochemical reaction," *Journal of the Electrochemical Society*, vol. 144, no. 6, pp. 1949–1952, 1997.

[20] S. Peulon and D. Lincot, "Mechanistic study of cathodic electrodeposition of zinc oxide and zinc hydroxychloride films from oxygenated aqueous zinc chloride solutions," *Journal of the Electrochemical Society*, vol. 145, no. 3, pp. 864–874, 1998.

[21] M. Izaki, T. Shinagawa, K. T. Mizuno, Y. Ida, M. Inaba, and A. Tasaka, "Electrochemically constructed p-$Cu_2O$/n-ZnO heterojunction diode for photovoltaic device," *Journal of Physics D: Applied Physics*, vol. 40, no. 11, article 010, pp. 3326–3329, 2007.

[22] J. Katayama, K. Ito, M. Matsuoka, and J. Tamaki, "Performance of $Cu_2O$/ZnO solar cell prepared by two-step electrodeposition," *Journal of Applied Electrochemistry*, vol. 34, no. 7, pp. 687–692, 2004.

[23] S. S. Jeong, A. Mittiga, E. Salza, A. Masci, and S. Passerini, "Electrodeposited ZnO/$Cu_2O$ heterojunction solar cells," *Electrochimica Acta*, vol. 53, no. 5, pp. 2226–2231, 2008.

[24] M. Ichimura and H. Takagi, "Electrodeposited ZnO/SnS heterostructures for solar cell application," *Japanese Journal of Applied Physics*, vol. 47, no. 10, pp. 7845–7847, 2008.

[25] E. Fatas, R. Duo, P. Herrasti, F. Arjona, and E. Garcia-Camarero, "Electrochemical deposition of cds thin films on Mo and Al substrates," *Journal of the Electrochemical Society*, vol. 131, no. 10, pp. 2243–2246, 1984.

[26] K. L. Hardee and A. J. Bard, "Semiconductor electrodes. x. photoelectrochemical behavior of several polycrystalline metal oxide electrodes in aqueous solutions," *Journal of the Electrochemical Society*, vol. 124, no. 2, pp. 215–224, 1977.

[27] A. J. Nelson, C. R. Schwerdtfeger, S. H. Wei et al., "Theoretical and experimental studies of the ZnSe/$CuInSe_2$ heterojunction band offset," *Applied Physics Letters*, vol. 62, no. 20, pp. 2557–2559, 1993.

[28] K. P. Musselman, A. Marin, A. Wisnet, C. Scheu, J. L. MacManus-Driscoll, and L. Schmidt-Mende, "A novel buffering technique for aqueous processing of zinc oxide nanostructures and interfaces, and corresponding improvement of electrodeposited ZnO-$Cu_2O$ photovoltaics," *Advanced Functional Materials*, vol. 21, no. 3, pp. 573–582, 2011.